

A framework for simultaneous fit of QCD and BSM parameters with xFitter

Xiao-Min Shen^{a,1,2,3}, Simone Amoroso^{b,1}, Jun Gao^{c,2,3},
Katerina Lipka^{d,1,4}, Oleksandr Zenaiev^{e,5}

¹ Deutsches Elektronen-Synchrotron DESY, Notkestr. 85, 22607 Hamburg, Germany

²INPAC, Shanghai Key Laboratory for Particle Physics and Cosmology, School of Physics and Astronomy, Shanghai Jiao-Tong University, Shanghai 200240, China

³Key Laboratory for Particle Astrophysics and Cosmology (MOE), Shanghai 200240, China

⁴Fakultät für Mathematik und Naturwissenschaften, Bergische Universität Wuppertal, Gaußstrasse 20, D-42119 Wuppertal, Germany

⁵Institute for Theoretical Physics, Hamburg University, Luruper Chaussee 149, 22761 Hamburg, Germany

Received: date / Accepted: date

DESY-24-119

Abstract An extension of the xFITTER open-source program for QCD analyses is presented, allowing for a polynomial parameterization of the dependence of physical observables on theoretical parameters. This extension enables simultaneous determination of parton distribution functions (PDFs) and new physics parameters within the framework of the Standard Model Effective Field Theory (SMEFT). The functionalities of the code are illustrated in a sensitivity study, where a simultaneous determination of the PDFs, top quark mass and the couplings of selected dimension-6 SMEFT operators is addressed using projections for measurements of top quark-antiquark pair production at the High-Luminosity LHC. The importance of considering all the correlations of the parton distributions, top quark mass and the SMEFT parameters in a simultaneous QCD+SMEFT analysis is demonstrated. This work serves as a new platform for simultaneous extraction of the PDFs and the SM/SMEFT parameters based on xFITTER.

Contents

1	Introduction	2
2	Framework on simultaneous fit of QCD and BSM	3
3	Extraction of SMEFT couplings from $t\bar{t}$ production	5
4	Results of joint SMEFT-PDF fits	11
5	Summary	16
A:	Installation and usage of the EFT reaction	18

^ae-mail: xiao-min.shen@desy.de

^be-mail: simone.amoroso@cern.ch

^ce-mail: jung49@sjtu.edu.cn

^de-mail: katerina.lipka@desy.de

^ee-mail: oleksandr.zenaiev@desy.de

1 Introduction

Investigating physics at the highest energy scales is one of the primary objectives of the physics program of the Large Hadron Collider (LHC) at CERN. Lack of direct evidence for new particles and interactions suggests that the scale of physics beyond the Standard Model (BSM) is higher than those probed directly at the LHC. However, the influence of fundamental new interactions could still show up indirectly through small deviations of experimental measurements from the SM predictions. The Standard Model Effective Field Theory (SMEFT) [1] provides a systematic framework for incorporating these higher-energy effects into low-energy theories, allowing for investigations of new physics phenomena in a controlled and organized approach. The SMEFT extends the SM Lagrangian \mathcal{L}_{SM} by a series of operators, $\mathcal{O}_i^{(d)}$ of dimensions $d > 4$, and effective couplings $c_i^{(d)} = C_i^{(d)}/\Lambda^{(d-4)}$ (Wilson coefficients), suppressed by appropriate powers of the energy scale Λ , at which the EFT low-energy approximation loses validity. Assuming lepton number conservation, the SMEFT Lagrangian may be written as

$$\mathcal{L}_{\text{SMEFT}} = \mathcal{L}_{\text{SM}} + \sum_i \frac{C_i^{(6)}}{\Lambda^2} \mathcal{O}_i^{(6)} + \dots \quad (1)$$

Constraints on these high-dimensional operators in the SMEFT framework have been derived by different groups using a variety of experimental data from the LHC. These analyses benefit greatly from the high energies achieved at the LHC, due to energy-dependent factors which amplify the impact of SMEFT operators on partonic cross sections. These interpretations of the LHC data rely on a detailed knowledge of the proton structure, described in terms of Parton Distribution Functions (PDFs) [2]. The PDFs cannot (yet) be calculated from the first principles and have to be determined using collider data itself, nowadays including also measurements from the LHC, and, in general, assuming no presence of BSM physics. Full consideration of the correlation between the SMEFT operators and the proton PDFs would potentially modify the constraints on both, PDFs and the SMEFT couplings. This correlation, however, has so far been disregarded in most but a few analyses [3, 4, 5, 6, 7, 8, 9]. In Ref. [3], for example, interplay between PDFs and EFT effects are accessed for high-mass Drell-Yan processes at the LHC. The necessity of joint PDF and EFT fit has also been studied using di-lepton invariant mass distribution and the forward-backward asymmetry in Drell-Yan processes in Refs.[9, 10], for top quark production in Refs.[5, 8], and for jet production in Refs.[4, 5]. The general conclusion of these investigations is that while the interplay between the PDFs and EFT effects remains moderate considering the current experimental precision, the combined SMEFT and PDF fit will be necessary for the interpretation of high-precision measurements at the High-Luminosity LHC (HL-LHC).

This work presents a development of a new public extension for simultaneous SMEFT and PDF fit within the open-source QCD analysis framework xFITTER [11, 12, 13], which has been widely used in experimental community for quantitative comparison of the data with theoretical predictions, determination of PDFs, fragmentation functions and SM parameters. Through its flexible and modular structure, xFITTER provides an interface to a number of programs providing PDF evolution, heavy flavour schemes, assumptions on the PDF parameterisation, and further theoretical inputs. Besides actual PDF fits within HERA and the LHC collaborations, the xFITTER framework has been used for extractions of SM parameters as electroweak mixing angle [14], the top quark mass m_t [15] or the strong coupling constant $\alpha_S(m_Z)$ [16] and to study effects of physics beyond the SM [10]. In Ref. [4] a simultaneous determination of $\alpha_S(m_Z)$, m_t and Wilson coefficients relevant for jet production [17] was performed. The interfaces used in these analyses to parameterise the cross section dependence on the studied parameters are, however, specific to the particular processes, parameters, and models used. In the present work, a new module of the xFITTER code is presented, which can be used for the determination of generic SM parameters and EFT couplings, possibly with a simultaneous extraction of the PDFs parameters. The advantage of this work with respect to earlier studies, e.g. those of Ref. [3], is that the EFT corrections are stored in fast grids, which incorporate the full PDF dependence and accurate quadratic EFT corrections.

The paper is organised as follows. In Sec. 2, the fit framework is introduced, together with a brief description of the targets of SM/EFT parameters determination in xFITTER. As an illustration of the

developed framework, a simultaneous SMEFT-PDF fit is performed, where the Wilson coefficients of selected dimension-6 SMEFT operators are determined together with the proton PDFs and the top quark pole mass, as discussed in Sec. 3 and Sec. 4. Conclusions are given in Sec. 5. The technical details of installation and using the code are given in Appendix A.

2 Framework on simultaneous fit of QCD and BSM

The cross section for a generic process at the LHC, binned with respect to an observable α , is factorised as:

$$\sigma^{(\alpha)}(\mathbf{c}; \alpha_s, \text{PDF}) = \sum_{a,b} \int dx_1 dx_2 f_a(x_1) f_b(x_2) \hat{\sigma}_{ab}^{(\alpha)}(\mathbf{c}; x_1, x_2, \alpha_s), \quad (2)$$

where $\mathbf{c} = (c_1, c_2, \dots)$ are BSM parameters to be fitted, α_s is the strong coupling constant, and $f_a(x)$ is the PDFs for a parton a , and $\hat{\sigma}_{ab}^{(\alpha)}$ are the corresponding parton-level cross sections. Details involving factorisation and renormalisation scales have been suppressed in Eq. (2) for simplicity. The BSM parameters, α_s , and the PDFs can be extracted (together or individually) from the experimental data $D^{(\alpha)}$ by minimizing the profiled log-likelihood function

$$\chi^2(\mathbf{c}, \alpha_s, \text{PDF}) = \sum_{\alpha, \beta=1}^{N_{\text{pt}}} (\sigma^{(\alpha)} - D^{(\alpha)}) [\text{cov}^{-1}]_{\alpha\beta} (\sigma^{(\beta)} - D^{(\beta)}), \quad (3)$$

where N_{pt} is the total number of data points used in the fit, and cov^{-1} is the inverse of the covariance matrix, incorporating both experimental and theoretical uncertainties. More details are given in e.g. [2]. Determination of BSM parameters and PDFs using the χ^2 method require both the precision and efficiency of the calculation of theoretical predictions $\sigma^{(\alpha)}$.

Higher-order perturbative corrections to the SM partonic cross sections are essential for determination of various SM backgrounds and therefore drive the sensitivity of searches for BSM physics at the LHC. Meanwhile, radiative corrections to the signal strength of BSM physics in $\hat{\sigma}(\mathbf{c}; \alpha_s)$ are equally important for accurate interpretation of the measurements and for constraining the BSM parameters. The QCD corrections to BSM effects in terms of SMEFT have been developed for a long time in decays of B mesons [18]. Later, similar approaches have been applied to calculations of next-to-leading order (NLO) QCD corrections in decays of the top quark [19, 20], as well as in production of top quarks [21, 22, 23, 24, 25] and jets [26, 27] at the LHC, induced by a subset of the SMEFT operators. Recently, automated tools have been developed for calculations of NLO QCD corrections to arbitrary hard processes including the contribution of all dimension-6 SMEFT operators [28]. These calculations and tools have been widely used in BSM searches at the LHC and lead to improved constraints on the Wilson coefficients of SMEFT operators.

At the same time, additional complications arise in performing joint global analyses of QCD and the BSM effects at the LHC. To incorporate the exact dependence of the theoretical predictions on the PDFs efficiently, fast-interpolation grid techniques [29, 30, 31], including PineAPPL grid [32], have been developed. In general, the computational expensive parton-level cross sections $\hat{\sigma}_{ab}^{(\beta)}(\mathbf{c}_0, x_1, x_2, \alpha_s)$ (for *fixed* BSM parameters \mathbf{c}_0) is decomposed by order in α_s , calculated once and stored in grids of parton flavors a, b , momentum fractions x_1, x_2 , and bin β , which can be later used in Eq. (2). Again, complexity related to factorisation and renormalisation scales is suppressed here for simplicity. Having incorporated dependence on coupling constants and renormalisation/factorisation scales, these grids, however, cannot handle also the cross section dependence on other SM parameters and the BSM parameters \mathbf{c} . To overcome this limitation, an implementation of dedicated analytic parameterisations, or development of interfaces to specific codes where the exact dependence can be implemented (either as tabulated data or using the grids) is necessary. This is for example the case for the CIJET [17] code, which allows to store and interpolate the contributions of certain SMEFT operators to the inclusive jet and dijet cross-sections via fastNLO-like grids [30, 31].

Fortunately, the dependence of observable on additional SM parameters or the BSM parameters \mathbf{c} can often be well described by a quadratic polynomial in the region concerned. As an example, the cross sections of many processes depend on Wilson coefficients of dimension-6 SMEFT operators quadratically at NLO in QCD, if the renormalisation group running effects can be omitted, as is the case discussed in Sec. 3,

$$\sigma(\mathbf{c}) = \sigma_{\text{SM}} + \sum_i \frac{C_i}{\Lambda^2} \sigma_i + \sum_{i,j} \frac{C_i C_j}{\Lambda^4} \sigma_{i,j} + \cdots \quad (4)$$

The assumption of quadratic dependence may also work well for the SM parameters. In the presented work, a specific case of the top quark mass m_t is discussed. Even though the measured observable is in general a complicated function of m_t , its dependence on m_t in the region of interest (e.g for $m_t = 172.5 \pm 4.0$ GeV) can often be well approximated by a quadratic polynomial as

$$\sigma(m_t = 172.5 \text{ GeV} + \delta m_t) = \sigma(m_t = 172.5 \text{ GeV}) + \sigma_{\delta m_t} \times \delta m_t + \sigma_{\delta m_t, \delta m_t} \times (\delta m_t)^2, \quad (5)$$

where $\sigma_{\delta m_t}$ and $\sigma_{\delta m_t, \delta m_t}$ are the linear and quadratic coefficients, respectively. Upon this observation, a general solution for the aforementioned problem is discussed in the present work and its implementation in xFITTER in terms of a new xFITTER module (so called **EFT reaction**) is documented.

To be specific, the xFITTER **EFT reaction** for a fit to a set of SM and/or BSM parameters $\mathbf{c} = (c_1, c_2, \dots)$, assuming that the contributions of \mathbf{c} to every fitted observable $\sigma^{(\alpha)}$ are well described by a polynomial of \mathbf{c} to quadratic¹ terms, is

$$\begin{aligned} \sigma^{(\alpha)}(\mathbf{c}; \alpha_s, \text{PDF}) &= \sigma_0^{(\alpha)}(\alpha_s, \text{PDF}) + \sum_i c_i \sigma_i^{(\alpha)}(\alpha_s, \text{PDF}) + \sum_{i \leq j} c_i c_j \sigma_{ij}^{(\alpha)}(\alpha_s, \text{PDF}) \\ &= \sigma_0^{(\alpha)} \left(1 + \sum_i c_i K_i^{(\alpha)} + \sum_{i \leq j} c_i c_j K_{ij}^{(\alpha)} \right). \end{aligned} \quad (6)$$

In the present work, the definition of \mathbf{c} is extended to include further SM parameters. The observables $\sigma^{(\alpha)}$ are not limited to cross sections and can be forward-backward asymmetries A_{fb} etc. The superscript α runs over all bins of all used datasets. Examples of SM/BSM parameters \mathbf{c} include SMEFT Wilson coefficients, and the shift of the top quark mass $\delta m_t = m_t - 172.5 \text{ GeV}$, also studied in Sec. 3. Corresponding linear and quadratic contributions are denoted by σ_i , and σ_{ij} , respectively, with $K_i = \sigma_i / \sigma_0$ and $K_{ij} = \sigma_{ij} / \sigma_0$ being the linear and quadratic K factors.

Besides the quadratic dependence assumption in Eq. (6), the xFITTER **EFT reaction** has barely limitation on the measured observables $\sigma^{(\alpha)}$ or fitted parameters \mathbf{c} . However, note that the linear/quadratic K factors or corrections σ_i, σ_{ij} have to be calculated separately prior to be used in the **EFT reaction**. These input K factors or theoretical predictions are usually calculated with a specific PDF set, neglecting their possible PDF dependence. In order to study the correlation between the PDFs and SM/SMEFT parameters, the xFITTER **EFT reaction** offers the option to read the linear/quadratic contributions σ_i, σ_{ij} from fast interpolation grids. To be specific, a set of fast interpolation grids corresponding to different choices of SM/BSM parameters $\{\sigma(\mathbf{c}_1), \sigma(\mathbf{c}_2), \dots\}$ should to be fed to the xFITTER **EFT reaction**, where a convolution of these grids with the PDFs is done, and the theoretical predictions for any \mathbf{c} are extracted by solving a system of linear equations. In this way, full PDF and SM/SMEFT dependence of the theoretical predictions is preserved during the fit. The details about the installation and usage of the xFITTER **EFT reaction** are given in Appendix A, where possibilities to include higher-power corrections beyond quadratic terms in Eq. (6) are also discussed.

In Refs. [7,8], the **SIMUnet** program is presented, which is an open-source tool for simultaneous fits of EFT and PDFs. It is built upon the NNPDF code, parameterizing PDFs using neural networks. The **SIMUnet** program makes use of the Monte Carlo replica method to propagate errors, and is currently limited to linear EFT corrections [7,33] via bin-by-bin K factors. Our work is based on the xFitter framework,

¹The limitation to quadratic interpolation is driven by a particular task to parametrise specific EFT couplings addressed, but the code can be extended to higher order polynomials.

which implies the χ^2 minimisation according to Eq. (3), and provides various PDF parameterisations. In our work, the EFT corrections are stored in fast grids, which incorporate the full PDF dependence and accurate quadratic EFT corrections.

3 Extraction of SMEFT couplings from $t\bar{t}$ production

The functionality and capabilities of the new EFT reaction is illustrated by a simultaneous determination of the PDFs, m_t , and the couplings of four relevant SMEFT operators in Eq. (7), using an HL-LHC projection for a measurement of the distribution of the invariant mass of the $t\bar{t}$ pair, $m_{t\bar{t}}$. In this analysis, the HL-LHC pseudo-data are used together with the combined HERA-I and II measurements of the inclusive deep-inelastic scattering (DIS) cross sections [34].

3.1 Theoretical predictions

Here, the selected dimension-6 SMEFT operators relevant for $m_{t\bar{t}}$ distribution and the calculation of the SMEFT cross sections used to extract the m_t and the Wilson coefficients are described. Furthermore, the PDF dependence of SMEFT linear/quadratic corrections is discussed, motivating the need to include the SMEFT corrections through fast-interpolation grids.

3.1.1 SMEFT operators

For BSM searches in the framework of SMEFT assuming lepton number conservation, the leading BSM contributions arise from dimension-6 SMEFT operators as in Eq. (1). In the present study, we consider the effect of the following operators relevant for $t\bar{t}$ production at the LHC:

$$\begin{aligned}
 O_{tu}^1 &= \sum_{i=1}^2 (\bar{t}\gamma_\mu t) (\bar{u}_i\gamma^\mu u_i) , \\
 O_{td}^1 &= \sum_{i=1}^3 (\bar{t}\gamma^\mu t) (\bar{d}_i\gamma_\mu d_i) , \\
 O_{tG} &= ig_s (\bar{q}_{L3}\tau^{\mu\nu} T^A t) \tilde{\varphi} G_{\mu\nu}^A + \text{h.c.} , \\
 O_{tq}^8 &= \sum_{i=1}^2 (\bar{q}_{Li}\gamma_\mu T^A q_{L,i}) (\bar{t}\gamma^\mu T^A t) .
 \end{aligned} \tag{7}$$

Here, t is the right-handed top quark, u_i, d_i are the right-handed quarks of the i -th generation, q_{Li} is the left-handed quark doublet of the i -th generation, φ is the Higgs doublet, $G_{\mu\nu}^A$ is the gluon field strength tensor, and g_s is the strong coupling. The associated Wilson coefficients $c_{tu}^{(1)}, c_{td}^{(1)}, c_{tG}, c_{tq}^{(8)}$ are assumed to be real numbers.

The limits on the addressed Wilson coefficients have been extracted in various works, with a few demonstrative examples listed below and summarised in the Table 1. The ATLAS collaboration [35] has reported marginalised 95% confidence level (CL) intervals on c_{tG} and $c_{tq}^{(8)}$, taking into account the linear EFT corrections at LO in QCD. Further, there are also limits extracted in the global fits. The SMEFiT collaboration [36] has imposed constraints to 50 dimension-6 SMEFT operators at NLO in QCD by fitting Higgs boson, diboson, and top quark production measurements at the LHC and electroweak precision observables from LEP and SLD. Both linear and quadratic corrections in the $1/\Lambda^2$ expansion are accounted for. The 95% CL limits for c_{tG} and $c_{tq}^{(8)}$ are also extracted by the Fitmaker group [37], by using the top quark, Higgs boson, diboson and electroweak measurements in a fit at leading order in QCD and considering linear EFT corrections only, not considering $c_{tu}^{(1)}$ and $c_{td}^{(1)}$, since only weak constraints can be obtained with linear EFT

contributions. The Wilson coefficients have also been constrained in the simultaneous SMEFT+PDF analysis in the CT18 global analysis framework [5] with additional top quark and jet production measurements at the LHC and the Tevatron, resulting in the limits at 90% CL, assuming $c_{tu}^{(1)} = c_{td}^{(1)}$. Further results based on the data used in NNPDF4.0 global analysis [38] are available, using SMEFT+PDF fit in the SIMUnet [7,8] framework and considering only linear EFT corrections.

	c_{tG} [TeV ⁻²]	$c_{tq}^{(8)}$ [TeV ⁻²]	$c_{td}^{(1)}$ [TeV ⁻²]	$c_{td}^{(1)}$ [TeV ⁻²]
ATLAS[35]	[-0.68, 0.21]	[-0.30, 0.36]	N/A	N/A
SMEFiT3.0[36]	[0.019, 0.180]	[-0.467, 0.208]	[-0.198, 0.186]	[-0.159, 0.139]
Fitmaker [37]	[0.12, 0.6]	[-13, 2.2]	N/A	N/A
CT18[5]	$-0.10^{+0.26}_{-0.30}$	$-0.8^{+2.58}_{-2.38}$	$0.14^{+0.61}_{-0.97}$	$= c_{tu}^{(1)}$

Table 1: Current limits on the Wilson coefficients obtained by ATLAS, SMEFiT, Fitmaker, and CT18 collaborations. The results of ATLAS, SMEFiT, Fitmaker are the marginalised intervals correspond to 95% CL, while the results of CT18 are at 90% CL.

3.1.2 Calculations of the theoretical predictions

The theoretical predictions for $t\bar{t}$ production in SM are calculated at NNLO in QCD using **MATRIX** [39,40] interfaced to **PineAPPL** [32]. The nominal value of the top quark pole mass is set to $m_t=172.5$ GeV. Predictions with m_t values of 167.5, 170, 175, 177.5 GeV are further generated to interpolate the m_t dependence. The renormalization and factorisation scales are set to $\mu_F = \mu_R = H_T/4$, with $H_T \equiv \sqrt{m_t^2 + p_{T,t}^2} + \sqrt{m_t^2 + p_{T,\bar{t}}^2}$.

The EFT corrections are calculated at NLO in QCD using Madgraph5_aMC@NLO [41] together with the SMEFT@NLO [28] model, using the same dynamical renormalisation and factorisation scales as in the SM predictions. The **PineAPPL** grids with various non-vanishing c_{tG} , $c_{tq}^{(8)}$, $c_{tu}^{(1)}$ and $c_{td}^{(1)}$ values are generated to account for both the linear and quadratic dependence. In this work, we omit the renormalisation group running² of the Wilson coefficients, as most of the other groups [3,5,7,8]. As a result, the theoretical predictions of the cross sections depend on these Wilson coefficients quadratically as in Eq. (6), such that these coefficients can be fitted by using the **xFITTER EFT** reaction. Though the EFT reaction can deal with the crossing terms between different the Wilson coefficients, these are not included in the present work for simplicity. For instance, corrections proportional to c_{tG}^2 are included, but not those from $c_{tG} \cdot c_{tq}^{(8)}$.

Predictions for the DIS reduced cross section are obtained at NNLO in QCD through QCDNUM [44] using the Thorne-Roberts [45,46,47] variable-flavor number scheme. The SMEFT operators considered in this work do not contribute to the DIS cross section at NLO in QCD.

3.1.3 Sensitivity of $m_{t\bar{t}}$ distributions to m_t and SMEFT coefficients

The values of m_t and of the SMEFT coefficients are treated as free parameters in the fit. In Fig. 1, the SM predictions for the $m_{t\bar{t}}$ distributions at NNLO in QCD, are shown for the values of m_t of 170, 172.5 and 175 GeV. The CT18NNLO PDF set [48] is used. The cross section exhibits largest sensitivity to the value of m_t in the first bin of $m_{t\bar{t}}$, close to the $2 \cdot m_t$ threshold region.

In Fig. 2, the m_t interpolation is illustrated, considering the cross section predictions in the first, second and last $m_{t\bar{t}}$ bins. The exact predictions are shown together with the linear, quadratic and cubic polynomial fits. While the the complete m_t range is used for linear and cubic fits, it is narrowed to $170 < m_t < 175$ GeV

²Renormalisation group running effects of the dimension-6 operators has been studied at LO in QCD for top quark production and Higgs boson production in Refs. [42,43], and at NLO in QCD for jet production in Ref. [4].

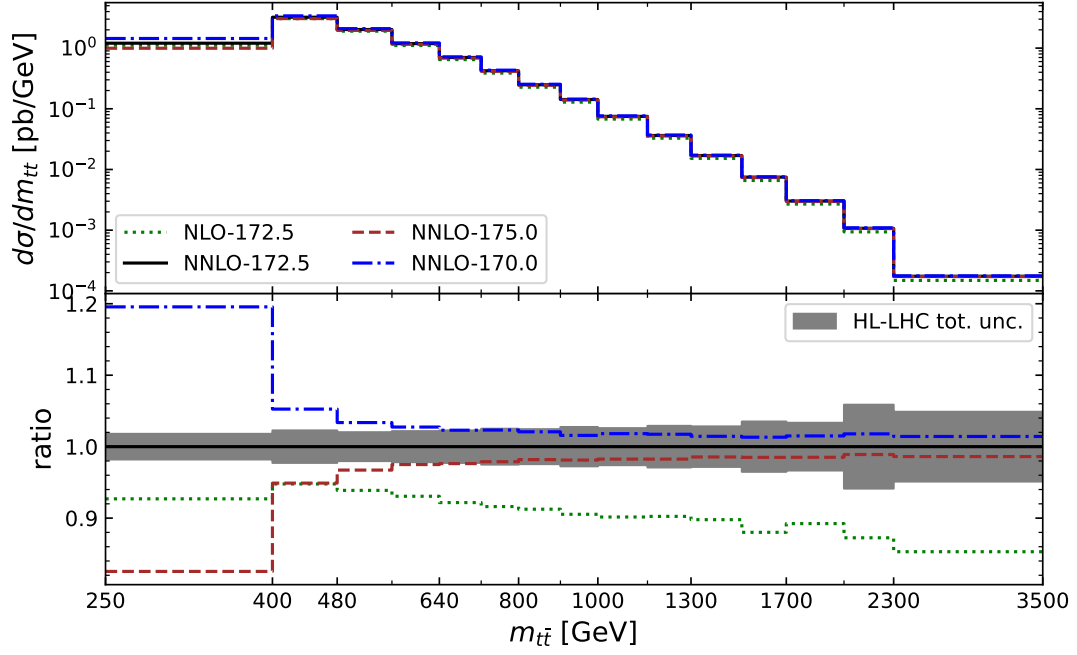


Fig. 1: The NNLO QCD prediction for $m_{t\bar{t}}$ distribution for $t\bar{t}$ production at the LHC at $\sqrt{s}=13$ TeV, assuming different values of m_t (lines of different styles). The projection for the total uncertainty in a future HL-LHC measurement (shaded band) is also shown.

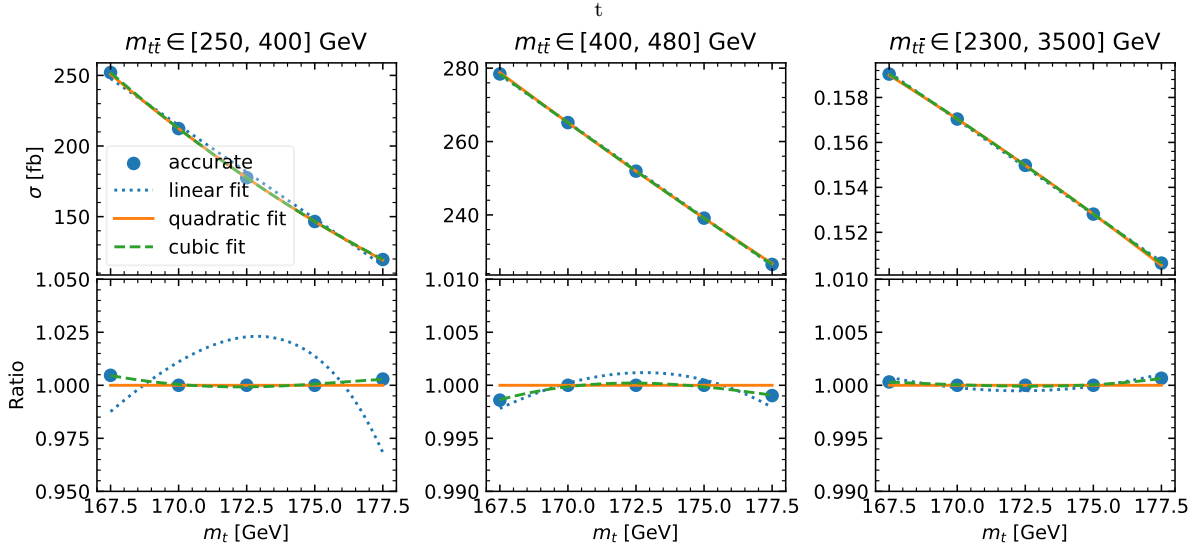


Fig. 2: The absolute (upper panel) and normalised (lower panel) dependence of the $t\bar{t}$ cross section prediction in selected $m_{t\bar{t}}$ bins on the value of m_t . The predictions obtained with $m_t=167.5, 170, 172.5, 175$ or 177.5 GeV, are shown by filled circles. The linear (dotted line), quadratic (solid line) and cubic (dashed line) polynomial interpolations are also shown.

for quadratic fit to achieve higher precision around 172.5 GeV. The corrections beyond quadratic power $\mathcal{O}(m_t - 172.5 \text{ GeV})^3$ are at per mill level for $m_t = 167.5, 177.5$ GeV. The missing higher power corrections are

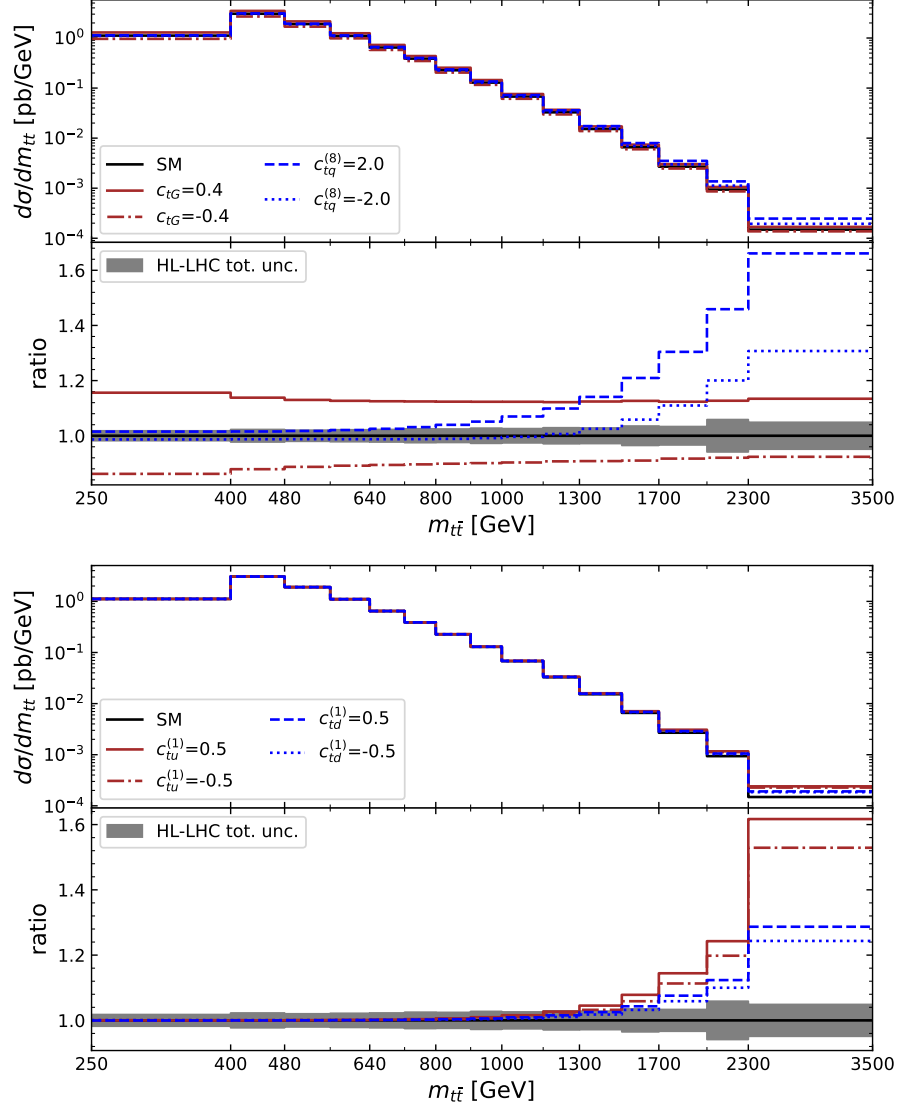


Fig. 3: Predictions for $m_{t\bar{t}}$ in SM and SMEFT at NLO in QCD, for different values of c_{tG} and $c_{tq}^{(8)}$ (upper) or $c_{tu}^{(1)}$ and $c_{td}^{(1)}$ (lower), shown by lines of different styles. The ratios are shown in the lower panels. In each SMEFT prediction, only one out of c_{tG} , $c_{tu}^{(1)}$, $c_{td}^{(1)}$, and $c_{tq}^{(8)}$ is considered non-zero for clarity. All the Wilson coefficients are shown in unit of TeV^{-2} . The projection for the experimental uncertainty in HL-LHC scenario is shown as a shaded band.

expected to be at $\sim 0.01\%$ level for $170 < m_t < 175$ GeV. In the following, the m_t dependence interpolated by the quadratic form is used within the EFT reaction as in Eq. (6).

The $m_{t\bar{t}}$ distributions assuming only one non-vanishing SMEFT parameter are shown in Fig. 3, together with the projection of the total experimental uncertainty expected at the HL-LHC. While the O_{tG} operator primarily modifies the overall $t\bar{t}$ production cross-section, the operators $O_{tq}^{(8)}$, $O_{tu}^{(1)}$ and $O_{td}^{(1)}$ mainly contribute to the cross section at high $m_{t\bar{t}}$. Also, for $|c_{tq}^{(8)}|$, $|c_{tu}^{(1)}|$ and $|c_{td}^{(1)}|$ around or larger than 0.5 TeV^{-2} , the quadratic corrections tend to dominate the linear ones and shall not be omitted in the fit.

From the theoretical predictions calculated for various non-vanishing SMEFT parameters, the linear and quadratic BSM K factors K_i and K_{ij} in Eq. (6) can be determined. In Fig. 4, the BSM K factors are presented. These are calculated by using ABMP16 [49], CT18 [48], MSHT20 [50], NNPDF4.0 [38] and HERAPDF2.0 [51] PDF sets, considering the PDF uncertainties at 68% CL. The factors $K_{tq8}^{(1)}$ and $K_{tq8}^{(2)}$, for example, correspond to the linear and quadratic BSM K factors of the Wilson coefficient $c_{tq}^{(8)}$, respectively. For c_{tG} , the PDF dependence of the BSM K factors is small. For $c_{tq}^{(8)}$, this dependence is much larger, as concluded from both, the individual PDF uncertainties and the differences in predictions obtained using different PDFs, reaching 20% at high $m_{t\bar{t}}$. This observation motivates using the fast interpolation grids to store the contribution of $c_{tq}^{(8)}$ instead of using BSM K factors derived with the fixed PDFs, in order to fully account for the correlation between PDFs and SMEFT parameters.

3.2 The datasets

In the present work, the combined HERA inclusive DIS cross sections [34] are used together with a projection for a future HL-LHC measurement of $t\bar{t}$ production as a function of $m_{t\bar{t}}$. The minimum Q^2 for the HERA DIS data is chosen to be 3.5 GeV^2 .

The HL-LHC pseudo-data are simulated using the same binning as used in a CMS measurement [52] of differential cross sections of $t\bar{t}$ production in the semileptonic decay channel using the Run 2 data at $\sqrt{s}=13 \text{ TeV}$. In particular, the same 15 bins of $m_{t\bar{t}}$ are used. The statistical uncertainties of Ref. [52] are scaled to their expectation values assuming an integrated luminosity of 3 ab^{-1} . Following the prescription of Ref. [53], the systematic uncertainties dominated by uncertainties in the b-jet calibrations and from theoretical modeling, are scaled down by a factor of two, while the uncertainty in the integrated luminosity of 1% is used. The nominal HL-LHC projection for the $m_{t\bar{t}}$ distribution corresponds to the SM theoretical predictions at NNLO in QCD with the value of $m_t=172.5 \text{ GeV}$, and using HERAPDF2.0NNLO [51]. Alternatively, a scenario is tested, where non-vanishing SMEFT contributions are present in the pseudo-data, obtained by adding the EFT corrections to the SM cross sections. In all the presented studies, the SM cross sections are calculated at NNLO in QCD, while the EFT corrections are calculated at NLO in QCD and assuming $c_{tG} = -0.1 \text{ TeV}^{-2}$ and $c_{tq}^{(8)} = 1.0 \text{ TeV}^{-2}$.

3.3 PDF parameterisation

The general strategy for a simultaneous QCD and BSM fit, introduced in Sec. 2, is used. The QCD analysis is performed at NNLO, with the DGLAP [54, 55, 56, 57, 58] evolution implemented in QCDNUM [44] version 18-00-00. QED corrections can be included into QCD evolution in the xFitter framework, but are neglected in this work since their effects are small for the processes under consideration. We also omit the impact of New Physics on the evolution of PDFs. The scale of New Physics in the SMEFT framework are assumed to be well above the electroweak scale, so new particles will not change radiations of QCD partons or the evolution of PDFs. The values of heavy quark masses are set as $m_c = 1.43 \text{ GeV}$ and $m_b = 4.5 \text{ GeV}$, while m_t is a free parameter of the fit. The value of $\alpha_S(m_Z)$ is set to 0.118. The PDF parameterisation corresponds to the one used in HERAPDF2.0 analysis [51]. The parameterised PDFs are the gluon $xg(x)$, the valence quark $xu_v(x)$ and $xd_v(x)$ distributions, as well as $x\bar{U}(x)$ for the up- and $x\bar{D}(x)$ for the down-type antiquarks. At the starting scale of QCD evolution $Q_0^2 = 1.9 \text{ GeV}^2$, the parameterisation form for a PDF f is

$$xf(x) = Af x^{B_f} (1-x)^{C_f} (1 + D_f x + E_f x^2). \quad (8)$$

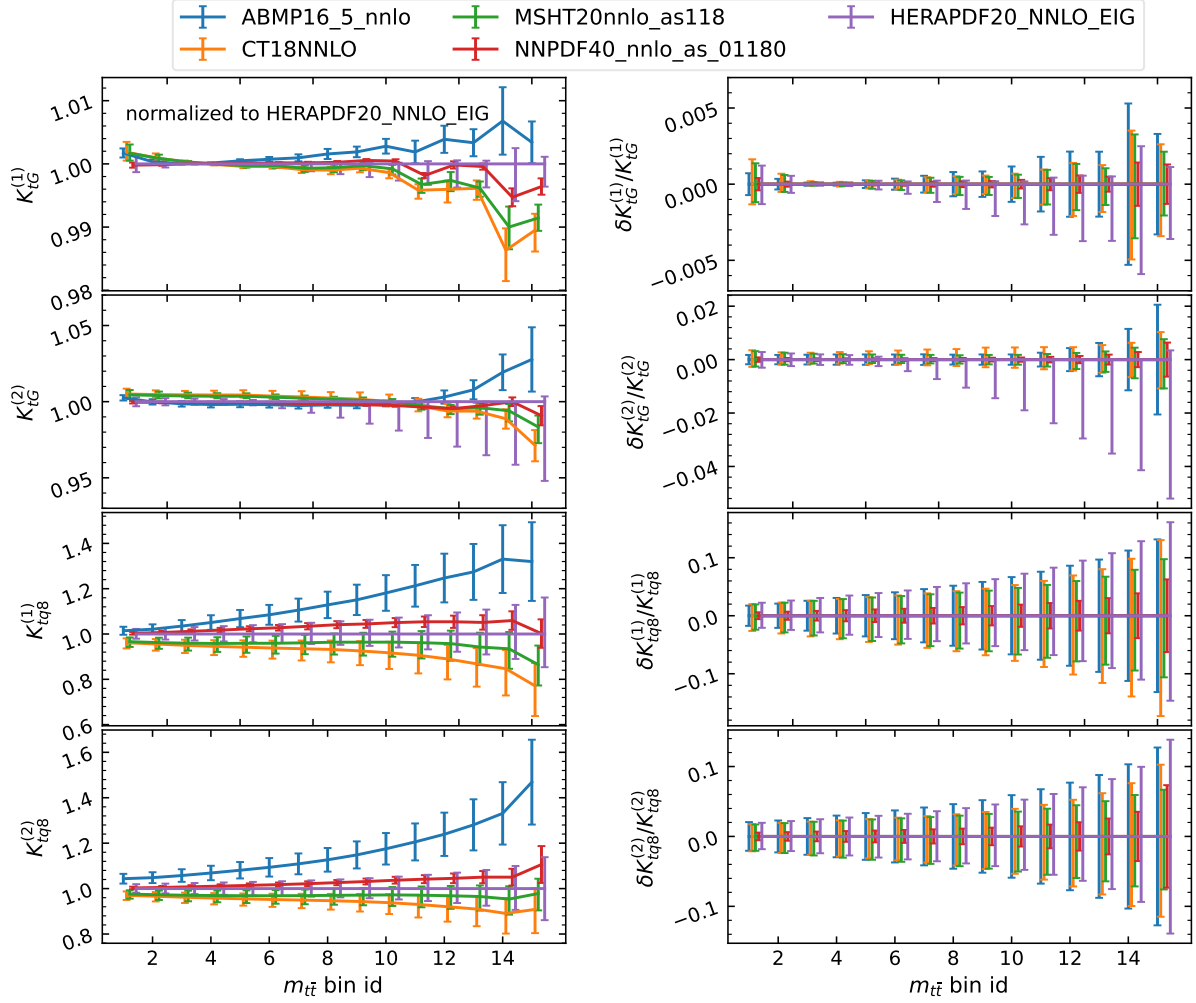


Fig. 4: The BSM K factors calculated with ABMP16, CT18, MSHT20, NNPDF40 and HERAPDF20 PDFs, together with the 68% CL PDF uncertainties in 15 $m_{t\bar{t}}$ bins as in Fig. 3, used in Ref. [52]. Shown are the linear and quadratic BSM K factors for c_{tG} and $c_{tq}^{(8)}$. Results in the left (right) panel are normalised to the central member of HERAPDF20 (individual PDF).

For the gluon distribution, an additional term of the form $A'_g x^{B'_g} (1-x)^{C'_g}$ is subtracted, allowing for a negative gluon at low x . The normalisation parameters A_{u_v} , A_{d_v} , and A_g can be determined from the QCD sum rules. The small- x behaviour of the PDFs is driven by the B parameters, whereas the C parameters are responsible for the behaviour as $x \rightarrow 1$. The relations $x\bar{U}(x) = x\bar{u}(x)$, $x\bar{s}(x) = f_s x\bar{D}(x)$, and $x\bar{d}(x) = (1 - f_s)x\bar{D}(x)$ are assumed at the starting scale, with $x\bar{u}(x)$, $x\bar{d}(x)$, and $x\bar{s}(x)$ being the distributions for the up, down, and strange antiquarks, respectively. Here, f_s is the strangeness fraction, fixed to $f_s = 0.4$ as in the HERAPDF2.0 analysis [51]. Further constraints $B_{\bar{U}} = B_{\bar{D}}$ and $A_{\bar{U}} = A_{\bar{D}}(1 - f_s)$ are imposed, so that the $x\bar{u}$ and $x\bar{d}$ distributions have the same normalisation as $x \rightarrow 0$. Note, that the xFITTER package interfaced with the EFT reaction is not bound to any particular parameterisation form.

Simultaneous fits of PDFs, m_t , and SMEFT Wilson coefficients are performed with xFITTER incorporating the xFITTER EFT reaction based on Eq. (6). The quadratic m_t dependence of the cross section is

adopted, as justified in Sec. 3.1.3. The PDF parameters, the value of m_t and the Wilson coefficients are extracted through minimisation of χ^2 , introduced in Sec. 2, applying a criterion of $\Delta\chi^2 = 1$. In the present study, only Hessian fit uncertainties are considered.

4 Results of joint SMEFT-PDF fits

Two alternative scenarios are considered in the present analysis, with respect to the generation of the $m_{t\bar{t}}$ pseudo-data. An SM scenario, where the pseudo-data do not contain any BSM effects, and a SMEFT scenario, where the $m_{t\bar{t}}$ pseudo-data include SMEFT contributions computed with $c_{tG} = -0.1 \text{ TeV}^{-2}$ and $c_{tq}^{(8)} = 1.0 \text{ TeV}^{-2}$, considering both linear and quadratic corrections. Besides investigating the correlations between the SM and SMEFT parameters, these scenarios can be used to hint to possible bias in the PDF extraction in case the data would indeed contain BSM physics, or, alternatively, test a BSM hypothesis in case no BSM physics is present. Note that DIS data from HERA, included for the PDF constraints, has no sensitivity to the value of m_t or the investigated Wilson coefficients. Given the illustrative character of the present analysis, no attempt was made to derive a complete and accurate set of parameter uncertainties. In particular, while uncertainties from the input data are derived using an Hessian approximation at the minimum, there was no attempt to estimate uncertainties from missing higher orders.

4.1 SM scenario for pseudo-data

The SM scenario mimics no BSM effects present in the $m_{t\bar{t}}$ distribution. The $t\bar{t}$ pseudo-data are generated using the SM NNLO QCD prediction with $m_t = 172.5 \text{ GeV}$, and using the HERAPDF2.0 NNLO PDF set. Two alternative fits are performed: in a fit denoted as *SM-SM*, the PDFs and m_t are fitted, while in a *SM-SMEFT* fit, the PDFs, m_t , and the coefficients $c_{tG}, c_{tq}^{(8)}, c_{tu}^{(1)}, c_{td}^{(1)}$ of the operators in Eq. (7) are obtained. The results are summarised in the Table 2 and are discussed in the following.

	m_t [GeV]	c_{tG} [TeV ⁻²]	$c_{tq}^{(8)}$ [TeV ⁻²]	$c_{tu}^{(1)}$ [TeV ⁻²]	$c_{td}^{(1)}$ [TeV ⁻²]
generated	172.5	0	0	0	0
SM-SM fit	172.53 ± 0.24	-	-	-	-
SM-SMEFT fit	172.51 ± 0.37	-0.01 ± 0.08	0.07 ± 0.62	-0.01 ± 0.42	0.00 ± 1.08

Table 2: Results for m_t and the Wilson coefficients obtained in the fits to HERA DIS and SM $m_{t\bar{t}}$ pseudo-data in the SM-SM and SM-SMEFT scenarios. The values in the first row correspond to the input parameters used to generate the pseudo-data.

SM-SM fit: The only difference between the present SM-SM fit and the original HERAPDF2.0 NNLO analysis [51] is the inclusion of the $t\bar{t}$ pseudo-data. While HERA DIS is not sensitive to the value of m_t , the $t\bar{t}$ data impose an additional constraint on the gluon distribution at high x , since the $t\bar{t}$ pairs are predominantly produced in gluon-gluon fusion, and probe m_t directly.

The PDFs extracted in the present SM-SM fit are compared to the original HERAPDF2.0 PDFs in Fig. 5. The difference between the central PDFs is negligible considering the fit uncertainties. The constraint on the gluon PDF improves at high x in SM-SM fit, attributed to inclusion of the $t\bar{t}$ pseudo-data, while only minor impact on the quark PDFs is observed. The value of the top quark pole mass in SM-SM fit is obtained as $m_t = 172.53 \pm 0.24 \text{ GeV}$, consistent with the input value of 172.5 GeV . Again, only the Hessian fit uncertainty is considered, which is compatible to the current uncertainty in m_t obtained in direct measurements at the

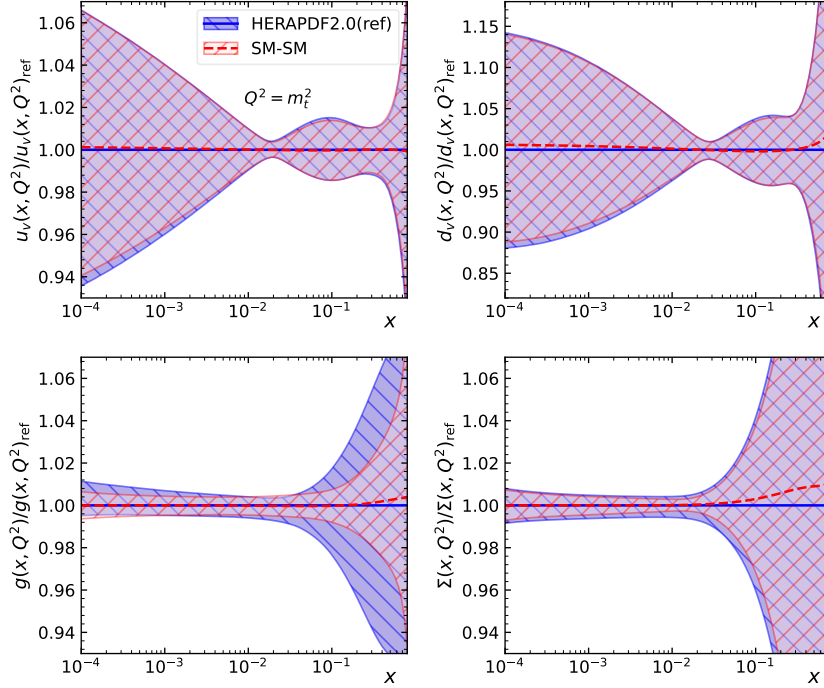


Fig. 5: The u_v , d_v , gluon and the sea PDFs obtained in the SM-SM fit (red shaded band), compared to the HERAPDF2.0NNLO PDFs [51] (blue shaded band), shown as a function of x at the factorisation scale of m_t . The distributions are divided by HERAPDF2.0 and the SM-SM result is shown by a dashed line).

LHC, e.g. the one of Ref. [59]. These results give confidence in the expectation that once the data contain only the SM contributions, the comprehensive QCD analysis would return the correct PDFs and the value of the SM parameters, in this example, m_t . While further uncertainties, e.g. arising from scale variations in the NNLO QCD predictions, will not change this conclusion, in an analysis based on real measurements these should be taken into account.

SM-SMEFT fit: In an alternative SM-SMEFT fit, an attempt is made to extract the BSM contributions from the data, where these are not present. In the SMEFT fit, both linear and quadratic corrections from SMEFT parameters are taken into account. In Fig. 6, the PDFs obtained in the SM-SM and SM-SMEFT fits are compared. The central values of the PDFs obtained in both fits almost coincide in the full x range. Minor difference ($< 5\%$) is observed for the quark PDFs in the large x region where PDF uncertainties are large. The uncertainties in the gluon PDF increase, once the SMEFT coefficients are added as free parameters in the fit, indicating a reduction of constraining power of the $t\bar{t}$ data due to correlation between the gluon PDF and SMEFT parameters. In the same way, the uncertainty in m_t increases. The results of the SM-SMEFT fit are consistent with the SM, with the obtained EFT coefficients consistent with zero, giving confidence that no fake signal of the new physics will be found in such a QCD analysis.

The SM-SMEFT fit is also useful to study the correlation between the gluon PDF and the values of m_t or SMEFT parameters. The PDFs extracted in the SMEFT+PDF fits, where the alternative values for $m_t=172.0$, 172.5 , or 173.0 GeV, are used, are presented in Fig. 7. Smaller value of m_t leads to reduction of the $t\bar{t}$ cross section close to the threshold, which would require larger contributions from the SMEFT coupling c_{tG} . To compensate for this effect at high $m_{t\bar{t}}$, the gluon PDF is reduced at large x . The PDFs

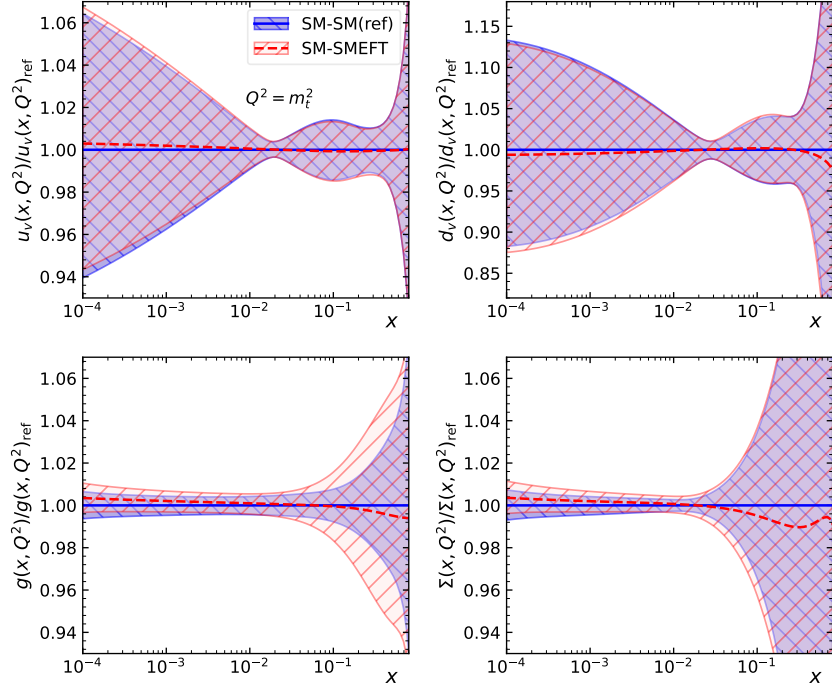


Fig. 6: The valence, the gluon and the sea PDFs with their uncertainties, obtained in the SM-SM fit (blue shaded band) and the SM-SMEFT fits (red shaded band), normalised to the results of SM-SM fit. The PDFs are shown as a function of x and the factorisation scale of m_t . The ratio of the results of the SM-SMEFT fit to those of SM-SM fit is presented by a dashed line.

extracted with alternative values of $c_{tG} = 0.0$ and 0.1 TeV^{-2} are shown in Fig. 8. For the same reason as in the case of varying m_t , the increase of c_{tG} leads to a reduction of the gluon PDFs at high x .

4.2 Fitting SMEFT pseudo-data

Here, a scenario is considered, where new physics is present in the pseudo-data of $t\bar{t}$ production of a future HL-LHC run. In particular, as detailed in Sec. 3.2, the pseudo-data is generated using the theoretical prediction assuming $c_{tq}^{(8)} = 1.0 \text{ TeV}^{-2}$, $c_{tG} = -0.1 \text{ TeV}^{-2}$, considering both linear and quadratic EFT corrections. For simplicity, the other SMEFT couplings are set to zero. Again, two general scenarios are considered. In a *SMEFT-SM* fit, only PDFs and m_t are fitted, attempting an SM-only interpretation of the data which do contain BSM effects. In the alternative *SMEFT-SMEFT* fit, the PDFs, m_t and the EFT coefficients are extracted simultaneously, correctly considering the generated BSM effects, and fully accounting for the correlations between EFT and SM parameters. The results are summarised in the Table 3 and are discussed in the following.

SMEFT-SMEFT fit: Here, the PDFs, m_t , and the SMEFT coefficients c_{tG} , $c_{tq}^{(8)}$, $c_{tu}^{(1)}$, $c_{td}^{(1)}$ are extracted simultaneously in a full SMEFT interpretation of the pseudo-data generated with non-zero assumption on c_{tG} and $c_{tq}^{(8)}$. The linear and quadratic corrections from SMEFT parameters are considered in the fit. The results, labelled as *SMEFT-SMEFT* in the Table 3, agree well with the truth values for all the inputs used to generate the pseudo-data, confirming that a comprehensive QCD analysis taking into account all the

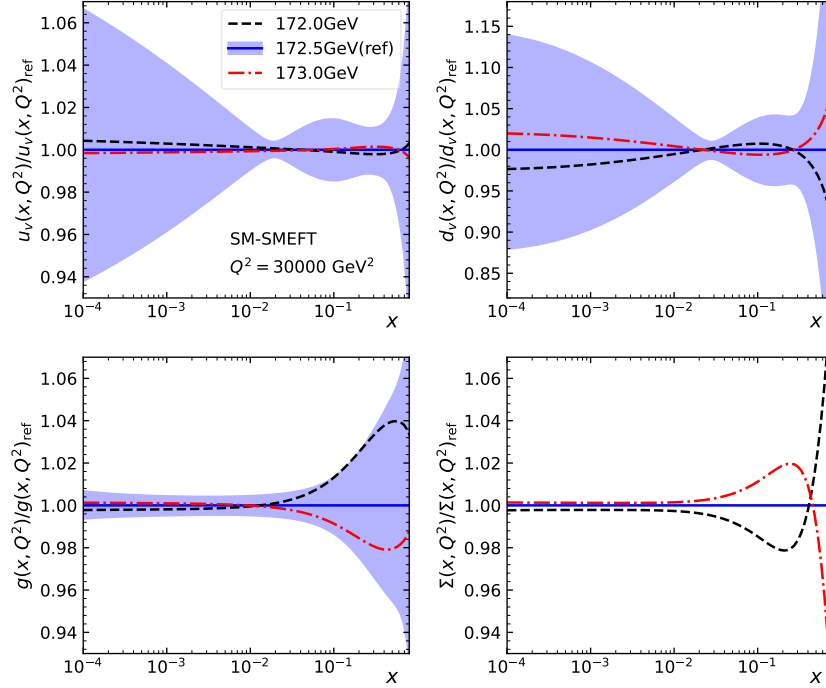


Fig. 7: Valence, gluon and sea PDFs obtained in SM-SMEFT fits assuming different values of m_t (lines of different styles), shown as functions of x at factorisation scale of 30000 GeV^2 . The PDF uncertainties (shaded bands) for the choice of $m_t = 172.5 \text{ GeV}$ are presented.

	m_t [GeV]	c_{tG} [TeV $^{-2}$]	$c_{tq}^{(8)}$ [TeV $^{-2}$]	$c_{tu}^{(1)}$ [TeV $^{-2}$]	$c_{td}^{(1)}$ [TeV $^{-2}$]
generated	172.5	-0.1	1.0	0	0
SMEFT-SMEFT (full)	172.50 ± 0.37	-0.11 ± 0.08	1.00 ± 0.25	-0.01 ± 0.37	0.01 ± 1.14
SMEFT-SMEFT (linear)	172.47 ± 0.36	-0.07 ± 0.39	0.35 ± 12.22	-0.35 ± 3.46	8.36 ± 53.34
SMEFT-SM	172.83 ± 0.23	-	-	-	-
fixed-PDF SMEFT	172.41 ± 0.35	-0.14 ± 0.08	0.93 ± 0.50	-0.01 ± 1.05	-0.09 ± 1.69

Table 3: Results for m_t and the Wilson coefficients obtained in the fits to HERA DIS and SMEFT $m_{t\bar{t}}$ pseudo-data using different scenarios. The values in the first row correspond to the input parameters used to generate the pseudo-data.

correlations among the SM and BSM parameters would return the correct result. The PDFs extracted in the present SMEFT-SMEFT fit are shown in Fig. 9.

Based on the result of the SMEFT-SMEFT fit, the correlation between the SM and EFT parameters is quantified in Fig. 10. In Fig. 10a, the correlations between m_t and c_{tG} are presented. The value of c_{tG} depends linearly on the assumed m_t . Once m_t and c_{tG} are considered as free parameters in the fit, both get constrained. Their correlation coefficient reaches $\rho_{m_t, c_{tG}} = 0.75$. This strong positive correlation is expected, since the increase of m_t reduces the cross sections close to the threshold $m_{t\bar{t}} \simeq 2m_t$, which can be compensated by requiring a larger value of c_{tG} . The correlation of m_t with $c_{tq}^{(8)}$, and of c_{tG} with $c_{tq}^{(8)}$ is shown in Fig. 10b and Fig. 10c, respectively. Resulting correlation coefficients are smaller, with $\rho_{m_t, c_{tq}^{(8)}} = 0.216$ and

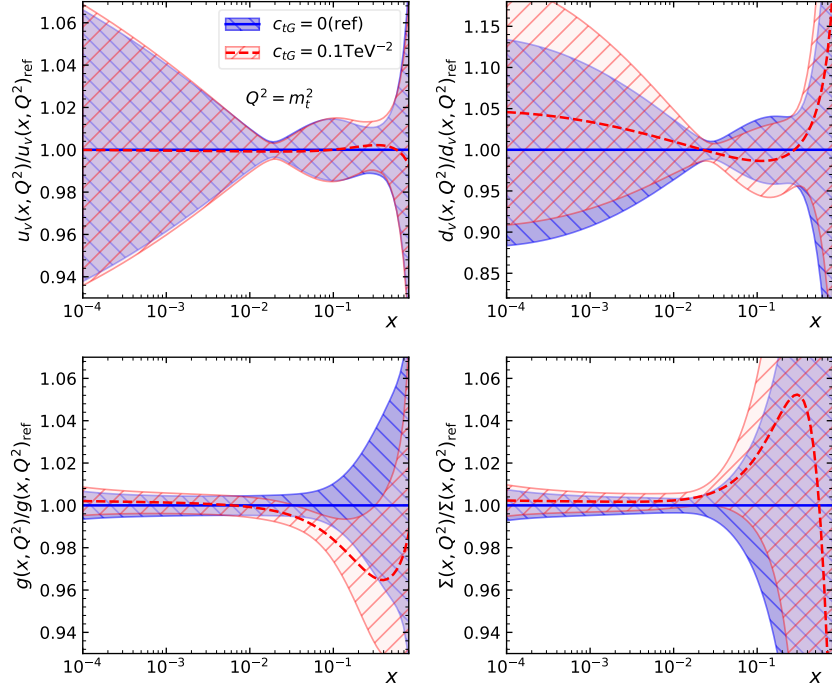


Fig. 8: PDFs extracted from SM-SMEFT fits with fixed values of $c_{tG} = 0$ and 0.1 TeV^{-2} , at a scale of $Q^2 = 30000 \text{ GeV}^2$.

$\rho_{c_{tG} c_{tq}^{(8)}} = 0.259$. That is expected because in contrast to m_t and c_{tG} , the coefficient $c_{tq}^{(8)}$ has only an impact on the cross sections at high $m_{t\bar{t}}$. The correlation between m_t and c_{tG} could possibly be mitigated (and the parameters better constrained) by using multi-differential distributions in $t\bar{t}$ production, e.g. as a function of $m_{t\bar{t}}$ and rapidity of the $t\bar{t}$ pair, or rapidity difference of the top quark and anti-quark. Of further advantage would be inclusion of the LHC measurements at different center of mass energies since these probe different composition of production channels via gluon fusion and quark annihilation.

The importance of the quadratic SMEFT corrections is estimated in a variant of the SMEFT-SMEFT fit, labelled as *SMEFT-SMEFT (linear)*, where only linear corrections are considered. As a result, the values of $c_{tq}^{(8)}$, $c_{tu}^{(1)}$ and $c_{td}^{(1)}$ are poorly constrained, as compared with the SMEFT-SMEFT full fit. This can be attributed to the fact that at high $m_{t\bar{t}}$, the quadratic SMEFT corrections are of the same size or even larger than the linear corrections.

SMEFT-SM fit: This study is performed in order to investigate potential bias in extracting the PDFs and m_t from the data, which potentially incorporate effects of new physics. In this case, the SM fit, assuming all the SMEFT coefficients to be zero, is performed using the SMEFT pseudo-data. In Fig. 9, the PDFs obtained from such a SMEFT-SM fit are shown and compared to the the correct SMEFT-SMEFT results. While the valence distributions from both fits are still compatible within their uncertainties, the gluon PDF obtained in SMEFT-SM fit is significantly different from the correct SMEFT-SMEFT solution at large x . This is caused by the actual presence of BSM physics in the $m_{t\bar{t}}$ pseudo-data, where the EFT $c_{tq}^{(8)}$ coupling contributes mostly to high invariant mass of the $t\bar{t}$ pairs, produced predominantly in gluon-gluon fusion, as illustrated in Fig. 3. At the same time, the uncertainties in the gluon PDF in the SMEFT-SM fit is underestimated at high x . The value of m_t is also shifted due to disregarded correlation with c_{tG} and the uncertainty is underestimated.

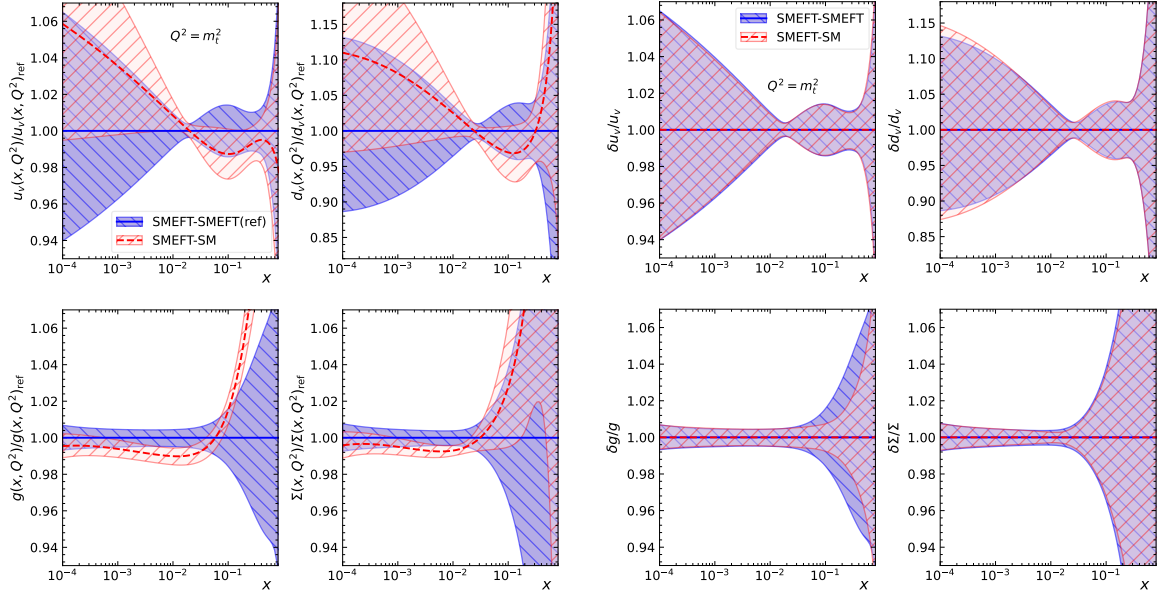


Fig. 9: The valence, the gluon and the sea PDFs (left panel) and their relative uncertainties (right panel), obtained in the SMEFT-SMEFT fit (blue shaded band) and the SMEFT-SM fit (red shaded band), shown as a function of x and the factorisation scale of m_t . The PDFs are normalised to the results of SMEFT-SMEFT fit and the ratio is presented by a dashed line.

SMEFT using fixed PDF: In an alternative analysis labelled as *fixed-PDF SMEFT*, we assume that no BSM effects are hidden in the data used for the PDF fit, while these are contained in the data used for the EFT interpretation. Instead of a full QCD+SMEFT analysis of DIS and HL-LHC pseudo-data, an EFT interpretation of the latter is performed, as often done in a conventional BSM search. In the focus of this investigations are the uncertainties in both PDFs and EFT coefficients. First, we extract PDFs from the QCD fit to the HERA DIS data only, which is equivalent to the HERAPDF20_NNLO_EIG PDF set [51]. This PDF set is then used in a SMEFT prediction to fit the values of m_t and SMEFT parameters, using the $t\bar{t}$ pseudo-data alone. The PDF uncertainties are taken into account by treating all the PDF eigenvectors as nuisance parameters. The results on m_t and SMEFT parameters are similar to those obtained in the SMEFT-SMEFT fit, however with increased uncertainties in $c_{tq}^{(8)}, c_{tu}^{(1)}, c_{td}^{(1)}$ coefficients. Therefore, using only low energy data in the PDF fit may help to avoid contamination by New Physics. However, the lack of high energy data leads to loose constraints on the resulting PDFs and the SMEFT parameters.

5 Summary

Uncertainties in the knowledge of the proton structure play an increasingly important role in the interpretation of the LHC measurements of Standard Model processes, requiring precise and unbiased determinations of SM or beyond SM (BSM) parameters to be performed simultaneously with a determination of PDFs.

This work presents a new module (so-called **EFT reaction**) for the xFITTER program for simultaneous extraction of PDFs and various SM/BSM parameters. The new EFT reaction provides a fast parameterisation of the cross-sections dependence on SM/SMEFT+PDF, incorporating both linear and quadratic SM/BSM corrections and considering the full dependence of these corrections on the PDFs. The EFT reaction can be also used for SM/SMEFT+PDF fits, or also for SM/BSM parameters extraction without fitting PDFs.

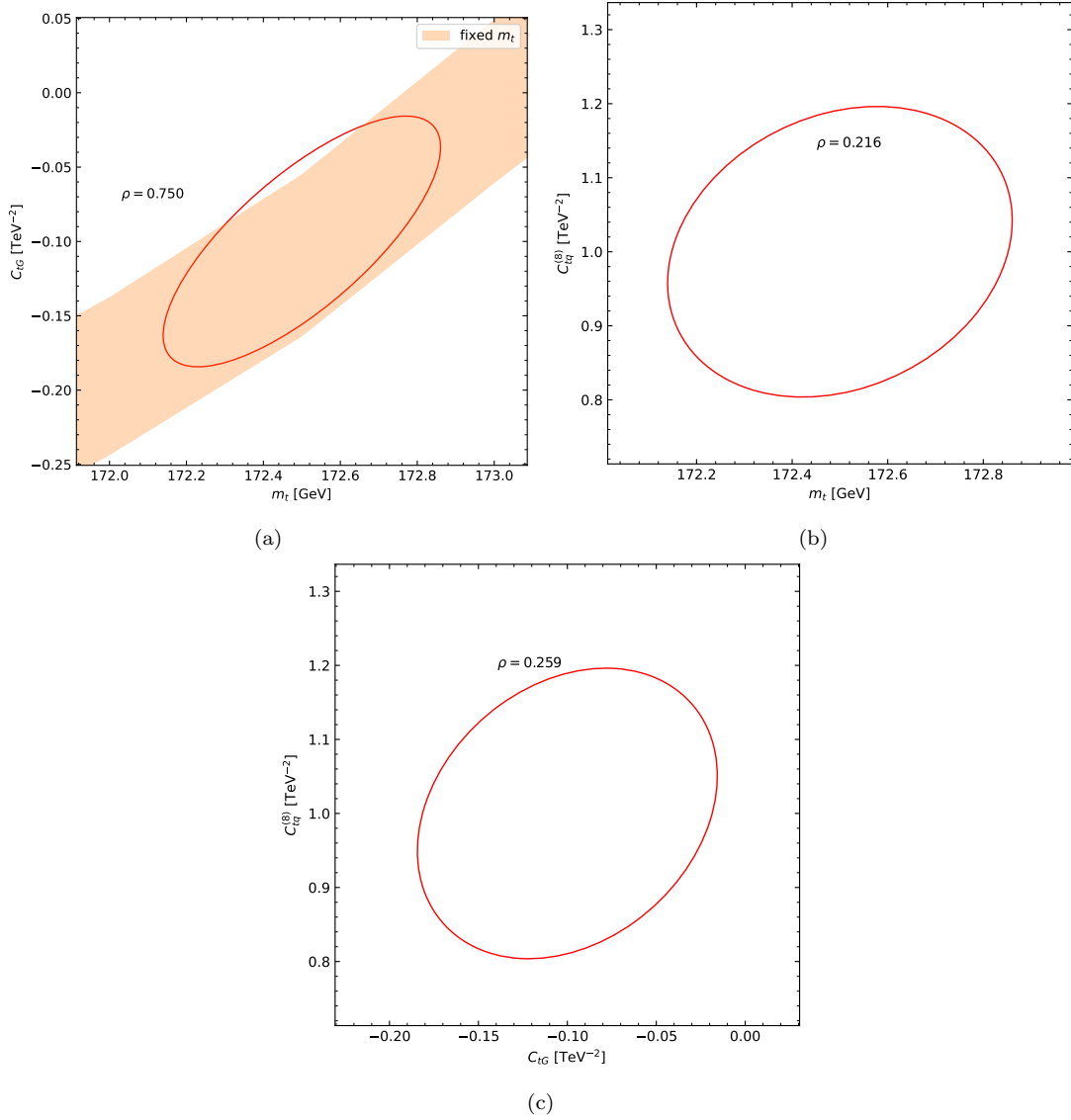


Fig. 10: Correlations between m_t and c_{tG} (panel a), m_t and $c_{tq}^{(8)}$ (panel b), and c_{tG} and $c_{tq}^{(8)}$ (panel c). The dependence of c_{tG} on an assumption on m_t is presented by the shaded band. In each panel, the ellipse represents the $\Delta\chi^2 = 1$ contour based on the Hessian matrix. The correlation coefficients ρ are also indicated.

The performance of the code is illustrated in an example exploring the sensitivity of $t\bar{t}$ production at the HL-LHC to selected operators in SM Effective Field Theory (SMEFT) framework. In particular, finite values for the EFT coefficients c_{tG} and $c_{tq}^{(8)}$ are assumed³ and the fits are performed in the Standard Model only and SMEFT scenarios. It is demonstrated that only careful consideration of the full correlations between PDFs, the value of m_t and the EFT parameters, including SMEFT quadratic corrections, would lead to the correct interpretation of the data. The correlations among the investigated parameters are also quantified.

³Alternatively, pseudo-data were generated with different values for c_{tG} and $c_{tq}^{(8)}$, which didn't modify any of presented conclusions.

The presented EFT reaction is offered as a new basis for SM/BSM+PDF interpretation of the measurements within the xFITTER framework, easily extendable to include arbitrary SM/SMEFT parameters and/or more datasets, according to the user case.

Acknowledgments

This work is supported by the Helmholtz grant W2-W3/123 and by the Helmholtz-OCPC Postdoctoral Exchange Program under grant No. ZD2022004. The work of JG is supported by the National Natural Science Foundation of China (NSFC) under Grant No. 12275173. The work of OZ is supported by the Philipp Schwartz-Initiative of the Alexander von Humboldt foundation. XS would like to thank Toni Mäkelä and Marco Guzzi for helpful discussions.

A: Installation and usage of the EFT reaction

For general installation and basic usage of xFITTER, the users will find it helpful to go through the documentation [60]. The xFITTER package is a powerful toolbox for extracting PDFs and α_s and incorporates various reactions for specific user cases. The AFB reaction [10] can be used to fit SMEFT parameters relevant for the forward-backward asymmetry A_{FB} . Quark contact interactions can be fitted using the CIJET reaction [4]. It is also possible to fit m_t to inclusive $t\bar{t}$ production rate data using the xFITTER interface to HATHOR [61]. The EFT reaction introduced in this work, on the other hand, aims to fit SM or EFT parameters for which a dedicated reaction is not yet available in the xFITTER. In the following, we will focus on the usage of the xFITTER EFT reaction.

The EFT reaction has been integrated into xFITTER, and is to be installed together with the main code. Users may also find it useful to adapt the examples in the `examples/EFT` directory to their physics case. For earlier versions of xFITTER, the EFT reaction may also be added by:

1. downloading the source code of the EFT reaction from the repository [62] and adding the EFT directory under `/path_to_xfitter/xfitter_master/reactions` ;
2. appending a new line `add_subdirectory(reactions/EFT)` to `/path_to_xfitter/xfitter_master/CMakeLists.txt` ;
3. recompiling xFITTER by executing

```
cd /path_to_xfitter
source setup.sh
cd xfitter_master
./make.sh install .
```

In order to consider the full correlation between PDFs and the other free parameters in the fit, the EFT reaction supports both APPLGRID [29] and PINEAPPL [32] fast-interpolation grids. If needed, the PINEAPPL package has to be installed within xFITTER, e.g. using the script from Ref. [63] and setting `skip_pineappl=0`.

The EFT reaction has barely limit on integration of the measured observables (e.g. differential cross sections, or A_{FB} etc.) and fitted parameters, except for the key assumption that the contributions of these parameters to the theoretical predictions for these observables can be well approximated by quadratic polynomials Eq. (6), which we quote here for readers' convenience

$$\begin{aligned}
\sigma^{(\alpha)}(\mathbf{c}) &= \sigma_0^{(\alpha)} + \sum_i c_i \sigma_i^{(\alpha)} + \sum_{i \leq j} c_i c_j \sigma_{ij}^{(\alpha)} \\
&\equiv \sigma_0^{(\alpha)} + \sum_i c_i l_i^{(\alpha)} + \sum_i c_i^2 q_i^{(\alpha)} + \sum_{i < j} c_i c_j m_{ij}^{(\alpha)} \\
&= \sigma_0^{(\alpha)} \left(1 + \sum_i c_i K_i^{(\alpha)} + \sum_{i \leq j} c_i c_j K_{ij}^{(\alpha)} \right), \tag{A.1}
\end{aligned}$$

where $l_i \equiv \sigma_i$, $q_i \equiv \sigma_{ii}$, $m_{i,j} \equiv \sigma_{i,j}$ denote the linear, quadratic, and mixed corrections, respectively. Consideration of cubic or even higher power corrections is discussed below.

The expression in Eq. (A.1) is the key input needed by the EFT reaction. For example, the last expression of Eq. (A.1) can be implemented in an xFITTER data file using the **TheorExpr** argument as

```
TermName      = 'SMNNLO',      'KEFT'
TermSource     = 'PineAPPL',    'EFT'
TermInfo       =
    'GridName=/path/to/PineAPPL_grid.pineappl',
    'ListEFTParam=deltamt,ctg,ctq8:FileName=/path/to/EFT_file.yaml
:xiF=1.0:xiR=1.0'
TheorExpr      = 'SMNNLO*KEFT'
```

where the theoretical prediction is the product of two terms, the SM prediction **SMNNLO** and a K factor **KEFT**. The **TermSource** designates the xFITTER reactions used to calculate the corresponding terms, and **TermInfo** provides variables passed to the reactions, separated by colons. In this example, the **SMNNLO** term is calculated by the **PineAPPL** reaction, with the path to the corresponding PineAPPL [32] grid given by keyword **GridName**. The **KEFT** term is a K factor calculated with the **EFT** reaction, whose ingredients we elaborate now.

Mandatory arguments for the EFT Term: There are two mandatory arguments for an EFT term. The argument **ListEFTParam** transmits to xFITTER the list of the SM/EFT parameters to be fitted⁴. As with other fit parameters in xFITTER, the initial values of the fit parameters $\{c_i\}$ shall be given in the **parameters.yaml** file. The corresponding BSM corrections, such as l_i, q_i, m_i, K_i in Eq. (A.1), are assumed to be provided in the **yaml** file, whose format is described below. The path to this EFT **yaml** file shall be given by the **FileName** argument.

Controlling the reaction output: By default, the EFT reaction returns the ratio $\sigma(\mathbf{c})/\sigma(\mathbf{c}=0)$, which may correspond to the BSM factor $\sigma_{\text{SM+EFT}}/\sigma_{\text{SM}}$. Here $\sigma(\mathbf{c})$ is the theoretical predictions corresponding to the current values of \mathbf{c} , which are updated from one iteration to another during the fit. This behavior can be changed by two optional arguments. One is the **AbsOutput** argument (**False** by default), which determines if the output shall be divided by the central predictions $\sigma(\mathbf{c}=0)$, and the other is the **NoCentral** argument (**False** by default), which toggles if the central contributions should present in the output. Outputs corresponding to different combinations are summarized in Table 4.

AbsOutput	NoCentral	reaction output
False	False	$\sigma(\mathbf{c})/\sigma(\mathbf{c}=0)$
False	True	$\sigma(\mathbf{c})/\sigma(\mathbf{c}=0) - 1$
True	False	$\sigma(\mathbf{c})$
True	True	$\sigma(\mathbf{c}) - \sigma(\mathbf{c}=0)$

Table 4: Outputs of the EFT reaction corresponding to different combinations of options.

Varying the scales: A common practice to estimate the effect of missing higher-order correction is to vary the renormalisation and/or factorisation scales by a factor $\xi_{R,F} \equiv \mu_{R,F}/\mu_{R,F}^{(0)}$, with $\mu_R^{(0)}$ ($\mu_F^{(0)}$) being the nominal scale choice in the generation of the fast-interpolation grids. This can be done with the **xiR** and **xiF** keywords in EFT reaction, (only applicable once the input linear/quadratic corrections are provided as APPLgrid or PineAPPL grids, instead of K factors).

⁴Note that the PDF parameters or $\alpha_s(m_Z)$ do not need to be declared in the **ListEFTParam** argument even if they are simultaneously fitted.

The EFT `yaml` file: As mentioned in Sec. 2, the linear and quadratic corrections $l_i, q_i, m_{i,j}$ in Eq. (A.1) have to be calculated outside xFITTER and fed to EFT reaction via an EFT `yaml` file. This EFT `yaml` file contains a list of entries, each corresponding to either of

- a linear/quadratic correction $(l_i, q_i, m_{i,j})$,
- a ratio (K_i, K_{ij}) , or
- a theoretical prediction $\sigma(\mathbf{c})$ (can be numbers or fast-interpolation grids) together with the values of \mathbf{c} .

Sufficient entries should be provided such that linear corrections l_i for all fitted parameters i (and also quadratic corrections $q_i, m_{i,j}$ if available) can be determined by solving a system of linear equations. Quadratic corrections $q_i, m_{i,j}$ that can not be extracted due to lack of necessary inputs are assumed to be zero.

As an example, an EFT `yaml` file of the form

```
# The EFT YAML file for fitting ctg
SM_NLO: # name of the entry is almost arbitrary
  type: C # Central predictions (sigma_0 in Eq.(A1))
  format: PineAPPL # xsec are PineAPPL tables
  xsec: [ /path/to/SM_NLO.pineappl ]
Linear_ctg: # This starts a new entry
  type: L # predictions up to Linear corrections
  param: ctg # name of the parameter (in ListEFTParam)
  param_value: 20.0 # value of ctg used to generate the grid
  format: PineAPPL
  xsec: [ /path/to/ctg1.pineappl ] # SM_NLO + 20.0*l_ctg
Quadratic_ctg: # SM_NLO + 40.0*l_ctg + 40.0^2*q_ctg
  type: Q # predictions up to Quadratic corrections
  param: ctg
  param_value: 40.0
  format: PineAPPL
  xsec: [ /path/to/ctg2.pineappl ]
```

can be used to fit the parameter `ctg`. This EFT `yaml` file has three entries, and the three involved grids provide the theoretical predictions (suppressing the units TeV^{-2} for simplicity),

$$\begin{aligned}\sigma(c_{tG} = 0) &\equiv \sigma_0 \\ \sigma_{\text{lin.}}(c_{tG} = 20) &= \sigma_0 + 20 \cdot l_{c_{tG}} \\ \sigma(c_{tG} = 40) &= \sigma_0 + 40 \cdot l_{c_{tG}} + 40^2 \cdot q_{c_{tG}}\end{aligned}\tag{A.2}$$

from which the EFT reaction extracts $l_{c_{tG}}$ and $q_{c_{tG}}$ and calculates the observable $\sigma(c_{tG})$ for any value of c_{tG} during the fit. For each entry in the above EFT `yaml` file, the theoretical predictions are given by the `xsec` node. The `type`, `param`, and `param_value` nodes work together to define the interpretation of `xsec`, as is summarized in Table 5.

The above EFT `yaml` file can be extended for extraction of c_{tq8} and the top quark mass m_t as follows.

```
# appended to the former EFT YAML file, to fit also ctq8 and mt
Quadratic_ctq8_1: # SM_NLO + 40*l_ctq8 + 40^2*q_ctq8
  type: Q
  param: ctq8
  param_value: 40.0
  #... inputs similar to Quadratic_ctg
Quadratic_ctq8_2: # SM_NLO + 30*l_ctq8 + 30^2*q_ctq8
  type: Q
  #... inputs similar to Quadratic_ctg
```

type	param	param_value	xsec
C	-	-	σ_0
l	i	-	$l_i \equiv \sigma_i$
q	i	-	$q_i \equiv \sigma_{ii}$
m	$[i, j]$	-	$m_{ij} \equiv \sigma_{ij}$
L	i	c_i	$\sigma_0 + c_i \sigma_i$
Q	i	c_i	$\sigma_0 + c_i l_i + c_i^2 q_i$
M	$[i, j]$	$[c_i, c_j]$	$\sigma_0 + c_i l_i + c_j l_j + c_i^2 q_i + c_j^2 q_j + c_i c_j m_{ij}$

Table 5: Possible `type`'s of the EFT `yaml` file entries, the needed `param`, `param_value` inputs, and the corresponding theoretical predictions (`xsec`), using the notation of Eq. (A.1). The theoretical predictions should be further divided by σ_0 if `format` node is set to `ratio`.

```
ctg_ctq8: # theoretical predictions for ctg=20, ctq8=40
  type: M # include the Mixing between ctg and ctq8
  param: [ctg, ctq8] # both ctg and ctq8 are non-zero
  param_value: [20.0, 40.0] # ctg=20, ctq8=40
  format: PineAPPL
  xsec: [ /path/to/ctg_ctq8.pineappl ]
Kfactor_mt_linear: # l_deltamt / Central
  type: l
  param: deltamt
  format: ratio # xsec is an array of ratios
  xsec: [-0.10349132, -0.02400355, -0.01317847, ... ]
```

This way, l_{ctq8} , q_{ctq8} , $m_{ctG,ctq8}$, and l_{m_t} can be fitted. The information about the quadratic corrections to m_t and the mixing term between m_t and the two SMEFT parameters, however, are missing and thus quadratic corrections $q_{\delta m_t}$, $m_{\delta m_t, ctG}$, $m_{\delta m_t, ctq8}$ will not be included in calculating the theoretical predictions.

We have shown in Fig. 4 that PDF dependence does not always cancel out completely in the BSM K factors, therefore the fast-interpolation grids are preferred to fully incorporate the correlation between the PDFs and SM/SMEFT parameters. However, when the number of EFT parameters to be fitted N is large, the number of involved fast-interpolation grids is also large ($O(N^2)$ for quadratic EFT fits or $O(N)$ for linear EFT fits). As a result, the calculation of theoretical prediction can be slow. For xFITTER EFT reaction, theoretical predictions can be either numeric (obtained for a particular choice of the PDF set) or fast-interpolation grids (essentially disentangled from the PDFs). This is indicated by the `format` node, which can be `PineAPPL` (`APPLgrid`) for the grids in `PINEAPPL` (`APPLGRID`) format, or by `xsection` for numerical values ($\sigma(c)$, σ_i or σ_{ij}), or `ratio` for ratios $K_i = \sigma_i/\sigma_0$, $K_{ij} = \sigma_{ij}/\sigma_0$, as is the case of `deltamt` in the above EFT `yaml` file.

Higher power corrections: To a limited extent, the cubic or even higher power corrections can be considered. As an example, corrections proportional to $(\delta m_t)^3$ and $c_{tG} \cdot (\delta m_t)^3$ can be provided via the following two entries with monomial type in the EFT `yaml` file:

```
# appended to the EFT YAML file above
mt_cubic: # contribution proportional to deltamt^3
  type: monomial
  format: ratio
  param: [deltamt]
  power: [3]
  xsec: [0.0001, ...]
mt3_ctg: # contribution proportional to deltamt^3 * ctg
```

```

type: monomial
format: ratio
param: [deltamt, ctg]
power: [3, 1]
xsec: [0.0002, ...]

```

For the cubic or higher power corrections, the current version of EFT reaction can only deal with corrections from monomials. Unlike **L**, **Q**, **M** entries in Table 5 or Eq. (A.2), these corrections can not be provided as linear combination of monomials.

References

1. I. Brivio and M. Trott, *The Standard Model as an Effective Field Theory*, *Phys. Rept.* **793** (2019) 1–98, [arXiv:1706.08945].
2. J. Gao, L. Harland-Lang, and J. Rojo, *The Structure of the Proton in the LHC Precision Era*, *Phys. Rept.* **742** (2018) 1–121, [arXiv:1709.04922].
3. A. Greljo, S. Iranipour, Z. Kassabov, M. Madigan, J. Moore, J. Rojo, M. Ubiali, and C. Voisey, *Parton distributions in the SMEFT from high-energy Drell-Yan tails*, *JHEP* **07** (2021) 122, [arXiv:2104.02723].
4. CMS Collaboration, A. Tumasyan et al., *Measurement and QCD analysis of double-differential inclusive jet cross sections in proton-proton collisions at $\sqrt{s} = 13$ TeV*, *JHEP* **02** (2022) 142, [arXiv:2111.10431]. [Addendum: JHEP **12**, 035 (2022)].
5. J. Gao, M. Gao, T. J. Hobbs, D. Liu, and X. Shen, *Simultaneous CTEQ-TEA extraction of PDFs and SMEFT parameters from jet and $t\bar{t}$ data*, *JHEP* **05** (2023) 003, [arXiv:2211.01094].
6. X.-M. Shen, J. Gao, M. Gao, T. J. Hobbs, and D. Liu, *Determining SMEFT and PDF parameters simultaneously based on the CTEQ-TEA framework*, *PoS EPS-HEP2023* (2024) 291.
7. Z. Kassabov, M. Madigan, L. Mantani, J. Moore, M. Morales Alvarado, J. Rojo, and M. Ubiali, *The top quark legacy of the LHC Run II for PDF and SMEFT analyses*, *JHEP* **05** (2023) 205, [arXiv:2303.06159].
8. M. N. Costantini, E. Hammou, Z. Kassabov, M. Madigan, L. Mantani, M. Morales Alvarado, J. M. Moore, and M. Ubiali, *SIMUnet: an open-source tool for simultaneous global fits of EFT Wilson coefficients and PDFs*, arXiv:2402.03308.
9. E. Hammou, Z. Kassabov, M. Madigan, M. L. Mangano, L. Mantani, J. Moore, M. M. Alvarado, and M. Ubiali, *Hide and seek: how PDFs can conceal new physics*, *JHEP* **11** (2023) 090, [arXiv:2307.10370].
10. A. Anataichuk et al., *Exploring SMEFT Couplings Using the Forward-Backward Asymmetry in Neutral Current Drell-Yan Production at the LHC*, arXiv:2310.19638.
11. S. Alekhin et al., *HERAFitter*, *Eur. Phys. J. C* **75** (2015), no. 7 304, [arXiv:1410.4412].
12. **xFitter Developers’ Team** Collaboration, V. Bertone et al., *xFitter 2.0.0: An Open Source QCD Fit Framework*, *PoS DIS2017* (2018) 203, [arXiv:1709.01151].
13. **xFitter** Collaboration, H. Abdolmaleki et al., *xFitter: An Open Source QCD Analysis Framework. A resource and reference document for the Snowmass study*, **6**, 2022. arXiv:2206.12465.
14. CMS Collaboration, *Measurement of the Drell-Yan forward-backward asymmetry and of the effective leptonic weak mixing angle using proton-proton collisions at 13 TeV*, tech. rep., CERN, Geneva, 2024.
15. M. V. Garzelli, J. Mazzitelli, S. O. Moch, and O. Zenaiev, *Top-quark pole mass extraction at NNLO accuracy, from total, single- and double-differential cross sections for $t\bar{t} + X$ production at the LHC*, arXiv:2311.05509.
16. ATLAS Collaboration, G. Aad et al., *A precise determination of the strong-coupling constant from the recoil of Z bosons with the ATLAS experiment at $\sqrt{s} = 8$ TeV*, arXiv:2309.12986.
17. J. Gao, *CIJET: A program for computation of jet cross sections induced by quark contact interactions at hadron colliders*, *Comput. Phys. Commun.* **184** (2013) 2362–2366, [arXiv:1301.7263].
18. G. Buchalla, A. J. Buras, and M. E. Lautenbacher, *Weak decays beyond leading logarithms*, *Rev. Mod. Phys.* **68** (1996) 1125–1144, [hep-ph/9512380].
19. J. J. Zhang, C. S. Li, J. Gao, H. Zhang, Z. Li, C. P. Yuan, and T.-C. Yuan, *Next-to-leading order QCD corrections to the top quark decay via model-independent FCNC couplings*, *Phys. Rev. Lett.* **102** (2009) 072001, [arXiv:0810.3889].
20. J. J. Zhang, C. S. Li, J. Gao, H. X. Zhu, C. P. Yuan, and T.-C. Yuan, *Next-to-leading order QCD corrections to the top quark decay via the Flavor-Changing Neutral-Current operators with mixing effects*, *Phys. Rev. D* **82** (2010) 073005, [arXiv:1004.0898].
21. J. Gao, C. S. Li, J. J. Zhang, and H. X. Zhu, *Next-to-leading order QCD corrections to the single top quark production via model-independent t-q-g flavor-changing neutral-current couplings at hadron colliders*, *Phys. Rev. D* **80** (2009) 114017, [arXiv:0910.4349].
22. J. Gao, C. S. Li, L. L. Yang, and H. Zhang, *Search for anomalous top quark production at the early LHC*, *Phys. Rev. Lett.* **107** (2011) 092002, [arXiv:1104.4945].
23. B. H. Li, Y. Zhang, C. S. Li, J. Gao, and H. X. Zhu, *Next-to-leading order QCD corrections to tZ associated production via the flavor-changing neutral-current couplings at hadron colliders*, *Phys. Rev. D* **83** (2011) 114049, [arXiv:1103.5122].

24. Y. Zhang, B. H. Li, C. S. Li, J. Gao, and H. X. Zhu, *Next-to-leading order QCD corrections to the top quark associated with γ production via model-independent flavor-changing neutral-current couplings at hadron colliders*, *Phys. Rev. D* **83** (2011) 094003, [arXiv:1101.5346].
25. D. Y. Shao, C. S. Li, J. Wang, J. Gao, H. Zhang, and H. X. Zhu, *Model independent analysis of top quark forward-backward asymmetry at the Tevatron up to $\mathcal{O}(\alpha_s^2/\Lambda^2)$* , *Phys. Rev. D* **84** (2011) 054016, [arXiv:1107.4012].
26. J. Gao, C. S. Li, J. Wang, H. X. Zhu, and C. P. Yuan, *Next-to-leading QCD effect to the quark compositeness search at the LHC*, *Phys. Rev. Lett.* **106** (2011) 142001, [arXiv:1101.4611].
27. J. Gao, C. S. Li, and C. P. Yuan, *NLO QCD Corrections to dijet Production via Quark Contact Interactions*, *JHEP* **07** (2012) 037, [arXiv:1204.4773].
28. C. Degrande, G. Durieux, F. Maltoni, K. Mimasu, E. Vryonidou, and C. Zhang, *Automated one-loop computations in the standard model effective field theory*, *Phys. Rev. D* **103** (2021), no. 9 096024, [arXiv:2008.11743].
29. T. Carli, D. Clements, A. Cooper-Sarkar, C. Gwenlan, G. P. Salam, F. Siegert, P. Starovoitov, and M. Sutton, *A posteriori inclusion of parton density functions in NLO QCD final-state calculations at hadron colliders: The APPLGRID Project*, *Eur. Phys. J. C* **66** (2010) 503–524, [arXiv:0911.2985].
30. T. Kluge, K. Rabbertz, and M. Wobisch, *FastNLO: Fast pQCD calculations for PDF fits*, in *14th International Workshop on Deep Inelastic Scattering*, pp. 483–486, 9, 2006. hep-ph/0609285.
31. **fastNLO** Collaboration, D. Britzger, K. Rabbertz, F. Stober, and M. Wobisch, *New features in version 2 of the fastNLO project*, in *20th International Workshop on Deep-Inelastic Scattering and Related Subjects*, pp. 217–221, 2012. arXiv:1208.3641.
32. S. Carrazza, E. R. Nocera, C. Schwan, and M. Zaro, *PineAPPL: combining EW and QCD corrections for fast evaluation of LHC processes*, *JHEP* **12** (2020) 108, [arXiv:2008.12789].
33. M. N. Costantini, M. Madigan, L. Mantani, and J. M. Moore, *A critical study of the Monte Carlo replica method*, arXiv:2404.10056.
34. **H1, ZEUS** Collaboration, H. Abramowicz et al., *Combination of measurements of inclusive deep inelastic $e^\pm p$ scattering cross sections and QCD analysis of HERA data*, *Eur. Phys. J. C* **75** (2015), no. 12 580, [arXiv:1506.06042].
35. **ATLAS** Collaboration, G. Aad et al., *Measurements of differential cross-sections in top-quark pair events with a high transverse momentum top quark and limits on beyond the Standard Model contributions to top-quark pair production with the ATLAS detector at $\sqrt{s} = 13$ TeV*, *JHEP* **06** (2022) 063, [arXiv:2202.12134].
36. E. Celada, T. Giani, J. ter Hoeve, L. Mantani, J. Rojo, A. N. Rossia, M. O. A. Thomas, and E. Vryonidou, *Mapping the SMEFT at High-Energy Colliders: from LEP and the (HL-)LHC to the FCC-ee*, arXiv:2404.12809.
37. J. Ellis, M. Madigan, K. Mimasu, V. Sanz, and T. You, *Top, Higgs, Diboson and Electroweak Fit to the Standard Model Effective Field Theory*, *JHEP* **04** (2021) 279, [arXiv:2012.02779].
38. **NNPDF** Collaboration, R. D. Ball et al., *The path to proton structure at 1% accuracy*, *Eur. Phys. J. C* **82** (2022), no. 5 428, [arXiv:2109.02653].
39. M. Grazzini, S. Kallweit, and M. Wiesemann, *Fully differential NNLO computations with MATRIX*, *Eur. Phys. J. C* **78** (2018), no. 7 537, [arXiv:1711.06631].
40. S. Catani, S. Devoto, M. Grazzini, S. Kallweit, and J. Mazzitelli, *Top-quark pair production at the LHC: Fully differential QCD predictions at NNLO*, *JHEP* **07** (2019) 100, [arXiv:1906.06535].
41. J. Alwall, R. Frederix, S. Frixione, V. Hirschi, F. Maltoni, O. Mattelaer, H. S. Shao, T. Stelzer, P. Torrielli, and M. Zaro, *The automated computation of tree-level and next-to-leading order differential cross sections, and their matching to parton shower simulations*, *JHEP* **07** (2014) 079, [arXiv:1405.0301].
42. R. Aoude, F. Maltoni, O. Mattelaer, C. Severi, and E. Vryonidou, *Renormalisation group effects on SMEFT interpretations of LHC data*, *JHEP* **09** (2023) 191, [arXiv:2212.05067].
43. F. Maltoni, G. Ventura, and E. Vryonidou, *Impact of SMEFT renormalisation group running on Higgs production at the LHC*, arXiv:2406.06670.
44. M. Botje, *QCDNUM: Fast QCD Evolution and Convolution*, *Comput. Phys. Commun.* **182** (2011) 490–532, [arXiv:1005.1481].
45. R. S. Thorne and R. G. Roberts, *An Ordered analysis of heavy flavor production in deep inelastic scattering*, *Phys. Rev. D* **57** (1998) 6871–6898, [hep-ph/9709442].
46. R. S. Thorne, *A Variable-flavor number scheme for NNLO*, *Phys. Rev. D* **73** (2006) 054019, [hep-ph/0601245].
47. R. S. Thorne, *Effect of changes of variable flavor number scheme on parton distribution functions and predicted cross sections*, *Phys. Rev. D* **86** (2012) 074017, [arXiv:1201.6180].
48. T.-J. Hou et al., *New CTEQ global analysis of quantum chromodynamics with high-precision data from the LHC*, *Phys. Rev. D* **103** (2021), no. 1 014013, [arXiv:1912.10053].
49. S. Alekhin, J. Blümlein, S. Moch, and R. Placakyte, *Parton distribution functions, α_s , and heavy-quark masses for LHC Run II*, *Phys. Rev. D* **96** (2017), no. 1 014011, [arXiv:1701.05838].
50. S. Bailey, T. Cridge, L. A. Harland-Lang, A. D. Martin, and R. S. Thorne, *Parton distributions from LHC, HERA, Tevatron and fixed target data: MSHT20 PDFs*, *Eur. Phys. J. C* **81** (2021), no. 4 341, [arXiv:2012.04684].
51. **H1, ZEUS** Collaboration, H. Abramowicz et al., *Combination of measurements of inclusive deep inelastic $e^\pm p$ scattering cross sections and QCD analysis of HERA data*, *Eur. Phys. J. C* **75** (2015) 580, [arXiv:1506.06042].
52. **CMS** Collaboration, A. Tumasyan et al., *Measurement of differential $t\bar{t}$ production cross sections in the full kinematic range using lepton+jets events from proton-proton collisions at $\sqrt{s} = 13$ TeV*, *Phys. Rev. D* **104** (2021), no. 9 092013, [arXiv:2108.02803].

-
53. P. Azzi et al., *Report from Working Group 1: Standard Model Physics at the HL-LHC and HE-LHC*, CERN Yellow Rep. Monogr. **7** (2019) 1–220, [[arXiv:1902.04070](#)].
 54. V. N. Gribov and L. N. Lipatov, *Deep inelastic $e p$ scattering in perturbation theory*, Sov. J. Nucl. Phys. **15** (1972) 438.
 55. G. Altarelli and G. Parisi, *Asymptotic freedom in parton language*, Nucl. Phys. B **126** (1977) 298.
 56. G. Curci, W. Furmanski, and R. Petronzio, *Evolution of parton densities beyond leading order: The non-singlet case*, Nucl. Phys. B **175** (1980) 27.
 57. W. Furmanski and R. Petronzio, *Singlet parton densities beyond leading order*, Phys. Lett. B **97** (1980) 437.
 58. S. Moch, J. A. M. Vermaseren, and A. Vogt, *The three-loop splitting functions in QCD: The nonsinglet case*, Nucl. Phys. B **688** (2004) 101, [[hep-ph/0403192](#)].
 59. CMS, ATLAS Collaboration, A. Hayrapetyan et al., *Combination of measurements of the top quark mass from data collected by the ATLAS and CMS experiments at $\sqrt{s} = 7$ and 8 TeV*, Phys. Rev. Lett. **132** (2024) 261902, [[arXiv:2402.08713](#)].
 60. “xFITTER main GIT repository.” <https://gitlab.cern.ch/fitters/xfitter/-/wikis/home>.
 61. M. Aliev, H. Lacker, U. Langenfeld, S. Moch, P. Uwer, and M. Wiedermann, *HATHOR: HAdronic Top and Heavy quarks crOss section calculatoR*, Comput. Phys. Commun. **182** (2011) 1034–1046, [[arXiv:1007.1327](#)].
 62. “GIT repository.” <https://gitlab.cern.ch/fitters/xfitter/-/tree/master/reactions/EFT>.
 63. “xFITTER installation script.” <https://gitlab.cern.ch/fitters/xfitter/-/raw/master/tools/install-xfitter>.